Boron doped small fullerenes C_{20}, C_{24}, C_{28} as a basis for the formation of heterostructures

Anton R. El Zanin[a], Sergey V. Boroznin[b], Irina V. Zaporotskova[c]

Volgograd State University, Volgograd, Russia

[a]aelzanin@volsu.ru, [b]boroznin@volsu.ru, [c]zaporotskova@volsu.ru

Corresponding author: A.R. El Zanin, aelzanin@volsu.ru

ABSTRACT In this paper, the stability, geometric and electronic properties of boron doped small fullerenes C_{20}, C_{24}, C_{28} were investigated using density functional theory (DFT) methods. Average bonds lengths were calculated and the stability of optimized structures was estimated. An analysis of one-electron spectra and the density of states (DOS) allowed us to define the mechanisms for the change in the band gap and to determine the dependence of this parameter on the concentration of boron atoms. The established dependence of the band gap on the concentration of impurity atoms suggests the possibility of controlling the refractive index of the considered nanomaterials by doping with different concentrations of boron atoms, which indicates the applicability of such an approach to the construction of heterostructures in general and photonic crystals in particular. The obtained results can be useful for the fabrication of the novel optoelectronic devices which are used in infocommunication systems for the manipulating and transformation of optical signals.

KEYWORDS small fullerenes, DFT, band gap, DOS, heterostructures, photonic crystals

1. Introduction

Improving the efficiency and reliability of information transmission systems is one of the most important vectors of the development of modern infocommunication technologies. Information transmission technologies using visible light as a signal carrier have become widespread. In this case, it is possible to implement a communication channel not only based on optical fiber, but also wirelessly, the so-called Li-Fi. Optical fiber technology, characterized by extremely high transmission capacity, the values of which can range from tens of Gbit/s to hundreds of Tbit/s [1–3], has now firmly entered the modern world. Li-Fi technology is only developing and is not so widespread yet, but it is high promising and is characterized by a sufficiently high transmission capacity and the possibility of application in air transport and medical facilities where Wi-Fi cannot be used cause of safety issues [4–6]. The above methods of information transmission, of course, require technical implementation using various optoelectronic devices. Heterostructures, and especially, photonic crystals, can be a basis for the construction of such devices, for example, optical switches [7,8], filters [9–14], logic adders and subtractors [15, 15–20], logic gates [21, 22].

Photonic crystals are structures characterized by a periodically (quasi-periodically) changing refractive index. The concept of a photonic band gap, analogous to the concept introduced to describe the behaviour of electrons in solids with a band gap, is used to describe the behaviour of photons in such structures. This corresponds to a certain range of wavelengths (frequencies), and photons with a wavelength (frequency) value within this range are unable to pass through a crystal [23–25]. The periodicity (or quasi-periodicity) of the refractive index changing determines the existence of such zones. The distinction between one-dimensional (1D), two-dimensional (2D) and three-dimensional (3D) photonic crystals is made on the basis of whether the refractive index changes along one, two or three orthogonal vectors (Fig. 1). It is also noteworthy that photonic crystals can be used to slow down optical pulses. Indeed, the speed of optical pulses can be reduced by more than 100 times [26, 27].

The selection of appropriate materials for heterostructures fabrication and the implementation of the technological process of its fabrication represent significant challenges. Carbon nanomaterials offer significant promise in this regard. Researchers have constructed different composites with the periodically changing properties using carbon nanotubes [28–34], graphene [35–41], and fullerenes [42–46]. These materials are advantageous, because structures with periodically changing physicochemical properties based on them can be obtained by doping different regions with impurity atoms. Boron atoms can act as an impurity, and this choice has a number of advantages: little distortion of the topology of the nanostructure due to a relatively small difference in the atomic radii of boron and carbon atoms, a significant effect of
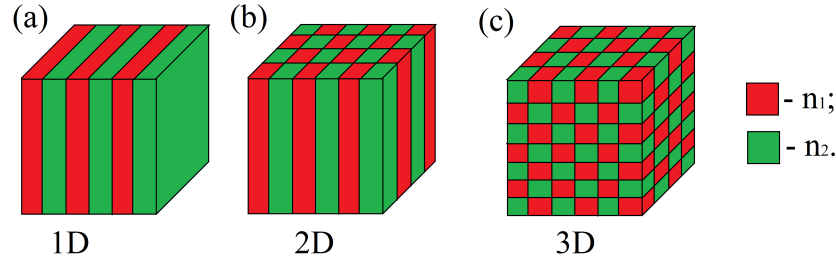
FIG. 1. Schematic illustration of one-dimensional (a), two-dimensional (b) and three-dimensional (c) photonic crystals consisting of two phases with different refractive indexes n_1 and n_2

even small amounts of impurity on the electronic properties of the material, and a well-established technology for doping carbon materials with boron atoms [47, 48].

In previous studies [49, 50], the concept of refractive index control was proposed. It is based on the relationship between the refractive index and the energy gap. By controlling the energy gap with the help of substituting boron atoms, it becomes possible to control the refractive index. The problem of the influence of substitution of carbon atoms by boron atoms in small fullerenes on electronic and optical properties is poorly studied. So, in the present work, we propose to consider the physicochemical properties of small fullerenes C$_{20}$, C$_{24}$, C$_{28}$ doped with boron atoms in the context of heterostructures fabrication.

2. Materials and methods

2.1. Description of the investigation objects

The investigation objects were small fullerenes C$_{20}$ with a point symmetry group I$_h$, C$_{24}$ with a point symmetry group D$_{6d}$, C$_{28}$ with a point symmetry group D$_2$. The concentrations of boron impurities were 15, 25 and 50 %. The structures corresponding to these concentrations were designated as BC$_5$, BC$_3$ and BC, respectively. The chosen concentrations are not arbitrary: a similar approach is widely used for planar and tubular carbon nanostructures [49–53].

It should be noted that the case under consideration is more specific in that neither graphene nor carbon nanotubes generally contain pentagons in their structure. The features of the structural characteristics of fullerenes lead to the deviation from the strictly defined structures BC$_5$, BC$_3$ and BC that are observed in boron-carbon nanolayers and nanotubes. It will be demonstrated subsequently that in BC$_5$ C$_{20}$ each boron atom is surrounded by either five or six carbon atoms; in the BC$_5$ nanotube, as indicated by the designation, there are precisely five carbon atoms around each boron atom. However, when defects (vacancies) are introduced into the graphene structure and pentagonal fragments are formed, it is possible to form fullerenes by convolution [54]. It is precisely due to this interconnectedness of various carbon nanostructures that it is possible to extend the approach previously used for graphene and carbon nanotubes to fullerenes. In certain instances, multiple variants of the mutual spatial arrangement of impurity atoms were contemplated, with the structures designated as Type A and Type B, respectively.

2.2. Details of the computer modeling

The study was carried out using the methods of DFT [55] at the level of theory B3LYP/6-31G. 6-31G basis set is widely used for computing structural and electronic properties of boron doped carbon nanostructures in modern studies [56, 57]. The initial fullerenes were optimized, after which part of the carbon atoms were replaced by boron atoms, and reoptimization was carried out. The geometry of the obtained structures was characterized by the average bond lengths C–C d_{C-C}, B–C d_{B-C} and B–B d_{B-B}. It was also calculated the value of the relative elongation of the C–C bond δd_{C-C}:

$$\delta d_{C-C} = \frac{d_{C-C}(\text{doped}) - d_{C-C}(\text{pure})}{d_{C-C}(\text{doped})} \cdot 100\%, \tag{1}$$

where $d_{C-C}(\text{doped})$ is an average length of the C–C bond in doped fullerene, $d_{C-C}(\text{pure})$ is an average length of the C–C bond in pure one.

Important for possible practical applications is the determination of the stability of boron doped fullerenes. The stability of the considered structures was evaluated by the bond energy E_b calculated by the formula

$$E_b = nE(C) + mE(B) - E(C_nB_m), \tag{2}$$

where $E(C)$ and $E(B)$ are the energies of the isolated carbon and boron atoms, n and m are the numbers of the carbon and boron atoms, $E(C_nB_m)$ is the energy of the fullerene.

The next step in the investigation is the evaluation of the possibility of refractive index control by doping selected small fullerenes with different concentrations of boron atoms. It should be noted here that the simplest way to change the refractive index n in the framework of this problem is to change the band gap. Thus

$$n^2 = \text{Re}\varepsilon + k^2, \tag{3}$$

where ε is the permittivity, k is the imaginary component of the complex refractive index, which is responsible for absorption.

The absorption α is determined by the conductivity of the sample σ according to the generally accepted formula:

$$\alpha = \sigma/cn\varepsilon_0, \tag{4}$$

where c is the speed of light and ε_0 is a permittivity of a vacuum. The relationship between conductivity and the band gap ΔE_g is well-known:

$$\sigma \sim \exp(-\Delta E_g/2k_B T), \tag{5}$$

where k_B is the Boltzmann constant, T is a temperature. All above described allows to control the refractive index of the nanostructures under consideration.

The band gap ΔE_g was estimated as the difference between energy of the lowest unoccupied molecular orbital E_{LUMO} (the bottom of the conduction zone) and the energy of the highest occupied molecular orbital E_{HOMO} (the maximum of the valence band):

$$\Delta E_g = E_{\text{LUMO}} - E_{\text{HOMO}}. \tag{6}$$

Such simple way of estimation of the band gap is suitable for heteroatom doped carbon nanostructures [58,59].

In the case of spin degeneration of electronic states, the energy values of molecular orbitals corresponding to both the spin-up state (alpha orbitals) and the spin-down state (beta orbitals) were considered. The band gap is calculated separately for each type of orbital. The one-electron spectra and DOS were constructed using the GaussSum program [60]. The analysis of the charge distribution was carried out on the basis of calculations of the values of atomic partial charges according to Mulliken [61].

It should be noted that the values of some estimated parameters for different types of structures corresponding to the same concentration of impurity atoms were not considered separately, but rather, their average values were taken. Therefore, if no indication is given that a parameter value pertains to a specific structure type (e.g., A or B), the value in question represents the average.

3. Results and discussion

3.1. Geometry and stability

Optimized geometries of the pure and doped small fullerenes C_{20}, C_{24}, C_{28} are represented in the Fig. 2.
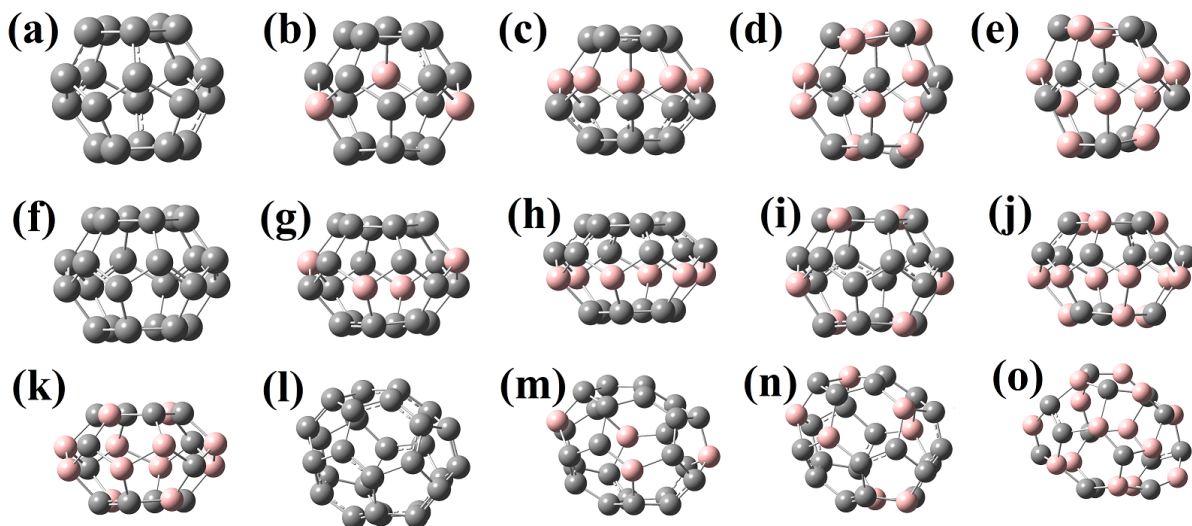

FIG. 2. Optimized geometries C_{20} (a), BC_5 C_{20} (b), BC_3 C_{20} (c), BC C_{20} type A (d), BC C_{20} type B (e), C_{24} (f), BC_5 C_{24} (g), BC_3 C_{24} type A (h), BC_3 C_{24} type B (i), BC C_{24} type A (j), BC C_{24} type B (k), C_{28} (l), BC_5 C_{28} (m), BC_3 C_{28} (n), BC C_{28} (o)

It was found that with the addition of 15 % of impurity atoms, the C–C bond length increases by 0.5 % in the case of fullerene C_{24}; for the rest of the considered fullerenes, this value practically does not change and the absolute value of the elongation is several hundredths of a percent or less. An increase in the concentration of boron atoms leads to a decrease in the average C–C bond length for C_{20} and C_{28} fullerenes, as evidenced by the monotonously decreasing nature of the dependence of the elongation on concentration and negative values of this value over the entire concentration range from 15 to 50 % (Fig. 3a). In the case of fullerene C_{24}, the elongation value is observed to lie in the positive region of the graph between 15 % and approximately 20 % of the concentration of boron atoms. Upon further increase in the concentration

of the impurity, the observed dependence is found to be consistent with that observed in the case of the other fullerenes under consideration. Based on the dependence of the average length of the B–C bond on the concentration of boron atoms (Fig. 3b), an increase in this indicator is observed with increasing concentration, reaching a maximum in the concentration range from 30 to 40 % of the impurity and then decreasing. Neighboring boron atoms take place only in BC structures, and the d_{B-B} parameter is only applicable to these. For BC C_{20} and BC C_{24} fullerenes, the average B–B bond length is on the order of 1.70 – 1.75 Å, depending on the type of structure. This value is 0.10 – 0.15 Å longer than the average B–C bond length and approximately 0.20 Å longer than the average C–C bond length in BC C_{20} and BC C_{24}. In BC C_{28} fullerene, the value of the average bond length of B–B is more than 2.60 Å, which is 1.00 – 1.20 Å longer than the average bond length of B–C and C–C in it. This is manifested in the appearance of octagons in the structure (Fig. 4), which, hypothetically, could facilitate the intercalation process of this kind of material by atoms and molecules. This is due to the fact that the potential barrier overcome by the particle during the intercalation process is lower for an octagon than for a pentagon or hexagon.
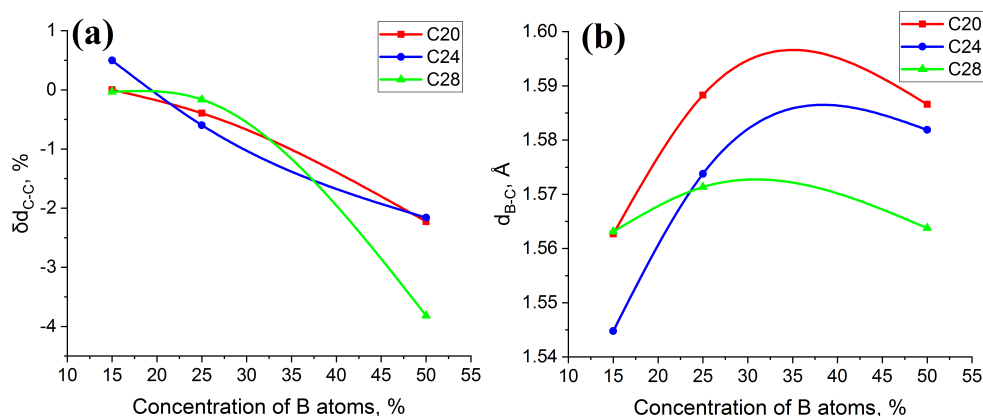

FIG. 3. The dependences of the relative elongation (a) and the average length of the B–C bond (b) on the concentration of boron atoms
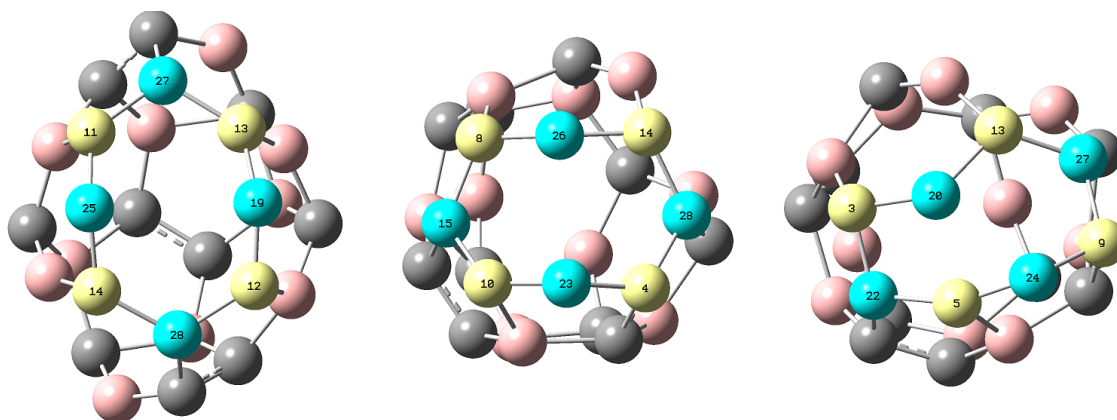

FIG. 4. Three octagons that take place in the BC C_{28} structure; atoms forming octagons are highlighted by yellow (carbon) and blue (boron) colors

Let us turn to the consideration of the stability of boron doped small fullerenes. The binding energy in such systems decreases monotonously with increasing impurity concentration (Fig. 5), respectively, pure fullerenes are more stable. However, the positive values of the binding energy over the entire concentration range under consideration indicate the possibility of their practical production, as well as the benefits of being in these states compared to being in the state of isolated carbon and boron atoms. Interestingly, the different spatial arrangement of boron atoms often has little effect on stability. The binding energies of different types corresponding to the same concentration differ by 0.22 – 0.43 %.

3.2. The influence of the concentration of the boron impurity on the band gap

Having considered the geometric and stability-related issues, we shall now turn our attention to the electronic properties of boron doped fullerenes. The following section will examine the relationship between the band gap of these nanostructures and the concentration of impurity atoms (Fig. 6).
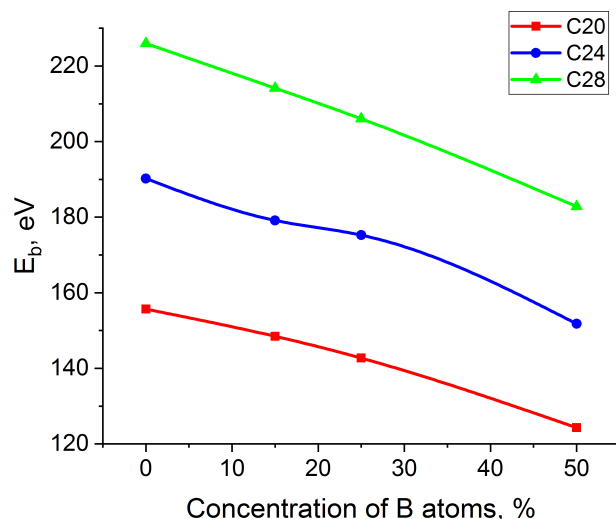
FIG. 5. The dependence of the binding energy on the concentration of boron atoms

In the case of fullerene C_{20}, the addition of 15 % of the impurity leads to an increase in the band gap to a value of 3.007 eV for the spin-up electronic states. For the spin-down states, an increase is also observed, but relatively small, by 0.126 eV compared to the initial structure. In the region of 15 % of the impurity concentration, the maximum value of the band gap is observed for both spin-up and spin-down states. In the range from 15 to 50 %, the function decreases monotonously. For the spin-up states, the band gap of the BC_3 C_{20} structure still has a greater value of the band gap compared to pure C_{20}; for the spin-down states, a different situation is observed – the band gap is smaller compared to the original structure. In BC C_{20} fullerenes of both types, the electronic states are non-degenerate in spin, respectively, the band gaps for the spin-up and spin-down states are identical. The addition of 50 % of the impurity leads to a decrease in the band gap compared to the initial fullerene by 0.195 – 0.316 eV, depending on the spatial arrangement of the atoms.

Consider the case of fullerene C_{24}. For the pure variant, the band gap is 1.864 eV. It is noteworthy that the electronic states for all its derivatives considered are non-degenerate in spin. The addition of 15 and 25 % of impurity boron atoms increases the band gap; the addition of 50 %, as in the case of C_{20}, leads to its decrease to values of 1.801 eV (for type A) and 1.531 eV (for type B), i.e. up to 1.666 eV, if we take the average value.

For fullerene C_{28}, spin degeneracy is observed only in the case of the BC_3 C_{28} structure. The addition of 15 and 50 % impurities of boron atoms makes it possible to decrease the band gap to values of the order of 1.30 eV. The addition of 25 % of the impurity leads to an increase of the band gap. The values of this parameter for the spin-up and spin-down states differ by 3.6 %.

3.3. Analysis of the one-electron spectra, DOS and PDOS

Following an overview of the general patterns of change in the band gap during doping of small fullerenes, it is essential to examine the processes occurring with the electronic structure in greater detail. The objective of this analysis is to examine the single-electron spectra and DOS for each nanosystem in greater detail.

Consider the case of fullerene C_{20}. The comparison is made with a pure structure (Fig. 7a). An increase in the band gap for the BC_5 C_{20} case (Fig. 7b) for the spin-up states is associated with an increase in the bottom of the conduction band of 0.314 eV and a decrease in the top of the valence band of 0.860 eV. For the spin-down states there is a decrease in the top of the valence band by 1.070 eV, but at the same time there is a decrease in the bottom of the conduction band by 0.944 eV – these two processes have opposite effects on the band gap. Thus, in spin-down states, a decrease in the bottom of the conduction band partially compensates for a decrease in the top of the valence band, so the increase in the band gap is not as significant as in spin-up states.

We will now proceed to examine the BC_3 C_{20} structure (Fig. 7c). In this case, two processes are observed for both the spin-up and spin-down states: a decrease of the top of the valence band and a decrease of the bottom of the conduction band. The values of the top of the valence band are essentially identical for the various types of states under consideration, with a maximum difference of approximately 0.10 %. The value of the conduction band bottom for spin-up states is 0.979 eV higher than that for spin-down states. The decrease in the bottom of the conduction band for spin-down states is greater in absolute value than the decrease in the top of the valence band, which ensures a decrease in the band gap compared to the initial structure. In contrast, for spin-up states, the decrease in the bottom of the conduction band
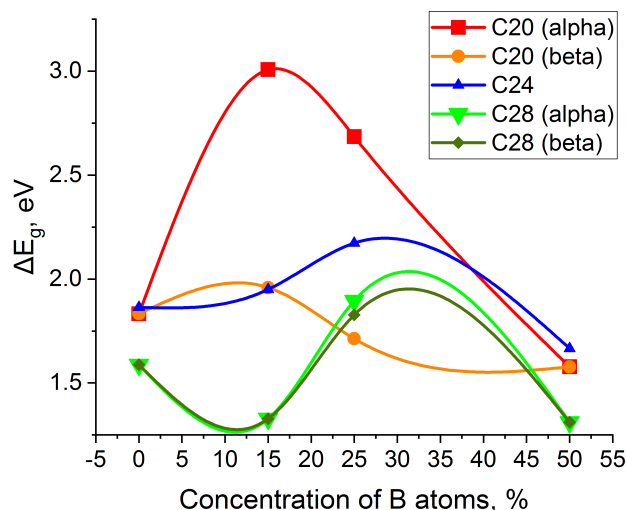
FIG. 6. The dependence of the band gap on the concentration of boron atoms; in the brackets it is the type of orbitals used for calculation of the band gap

is less significant in absolute value than the decrease in the top of the valence band, and therefore the band gap have the greater value than in pure C_{20}.

The qualitative mechanisms observed in the structures of fullerene C_{20} with a 50 % boron impurity (Fig. 7d,e) are analogous to those observed in the structures with a 25 % impurity. These include a decrease of the bottom of the conduction band and a decrease of the top of the valence band. However, in this case, the decrease in the bottom of the conduction band is fully compensated for by the decrease in the top of the valence band, resulting in a further narrowing of the band gap for both type A and type B structures. A comparison of the two structures reveals that the band gap of type A is 0.121 eV smaller than that of type B.

We now turn to materials based on fullerene C_{24} (Fig. 8). In the case of BC_5 C_{24} (Fig. 8b), there is an increase in the valence band top of 0.269 eV, while the bottom of the conduction band increases by 0.355 eV. Consequently, the band gap is observed to increase by 0.086 eV.

An increase in the impurity concentration to 25 % (Fig. 8c,d) results in an increase in the band gap to 2.130 eV for a type A structure and to 2.216 eV for a type B structure. In the case of a type A structure, there is an increase in the bottom of the conduction band and a relatively insignificant (approximately 0.30 %) decrease in the top of the valence band. It is evident that these processes are responsible for the observed increase in the band gap. In the case of a type B structure, a decrease is observed in both the bottom of the conduction band and the top of the valence band. A sufficiently large decrease in the top of the valence band by 0.511 eV results in an increase in the band gap. Conversely, a decrease in the conduction band bottom by 0.159 eV partially compensates for this.

The decrease in the band gap in BC C_{24} structures (Fig. 8e,f) is determined by a decrease in the bottom of the conduction band. The positions of the bottom of the conduction band in structures of type A and type B differ by 0.72 %, however, the band gaps differ by 17.6 %. This is due to a stronger decrease in the top of the valence band in the type A structure, while in the type B structure it is not so significant.

Further we will examine a number of different variants of boron doped fullerene C_{28} (Fig. 9). Upon doping C_{28} with 15 % of the impurity of boron atoms (Fig. 9b), the top of the valence band increases by 0.470 eV and the bottom of the conduction band increases by 0.210 eV. Therefore, the band gap is decreased by 0.260 eV. An increase in the band gap in the case of the BC_3 C_{28} structure (Fig. 9c) for both spin-up and spin-down states is associated with a more significant increase in the bottom of the conduction band relative to an increase in the top of the valence band. For the BC C_{28} structure (Fig. 9d), a decrease in the band gap is realized due to the same mechanisms as in the case of BC_5 C_{28}, i.e. due to a more significant increase in the top of the valence band relative to a smaller increase in the bottom of the conduction band. However, if in the case of BC_5 C_{28}, there was an increase in the bottom of the conduction band by 4.60 %, then here it was only by 0.62 %. At the same time, in the case of BC_5 C_{28}, there was an increase in the valence band top by 7.63 %, and in the case of BC C_{28} – by 4.95 %. As a result, the values of the band gap for structures with 15 and 50 % impurities differ slightly (by 1.28 %).

3.4. Charge distribution analysis

The analysis of the charge distribution showed that in all the considered cases, the electron density shifts from boron atoms to carbon atoms. A similar pattern also occurs for other carbon nanostructures: nanotubes [50] and nanolayers [51].
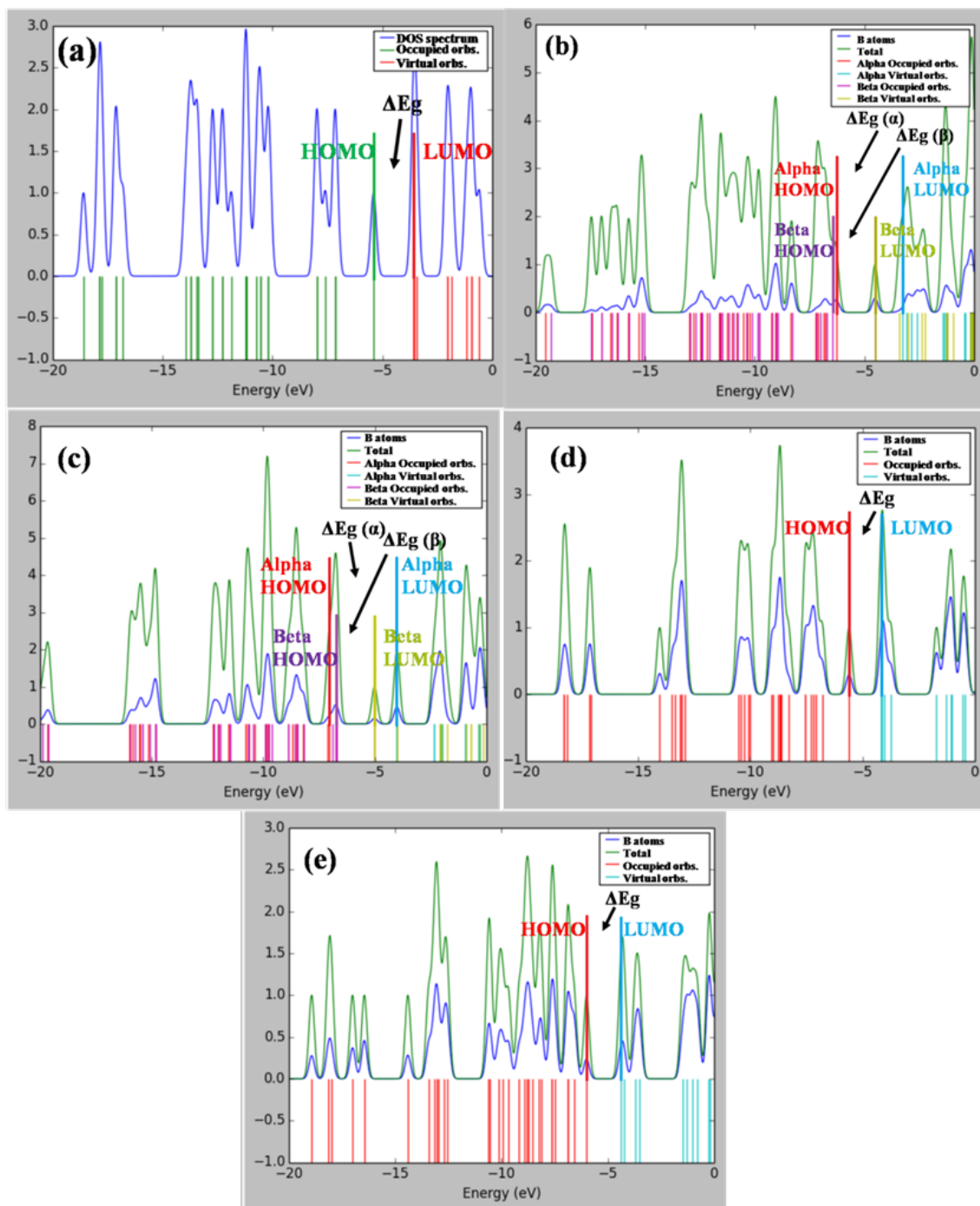
Fig. 7. One-electron spectra and total DOS of the C_{20} (a), total DOS (green curve) and partial DOS of boron atoms (blue curve) of the BC_5 C_{20} (b), BC_3 C_{20} (c), BC C_{20} type A (d), BC C_{20} type B (e)

We denoted the average charge on carbon atoms as $Q(C)$, on boron atoms – $Q(B)$. For the case of fullerene C_{20}, the maximum average charge on boron atoms is observed at an impurity concentration of 15 % and is 0.313; with increasing concentration, this indicator decreases monotonously. For BC C_{20} structures, the difference in the considered indicator for the two types is 1.7 %. The average charge on carbon atoms also decreases monotonously with increasing concentration, from -0.055 for BC_5 C_{20} to -0.242 for BC C_{20} type A and -0.238 for type B. For boron doped fullerene C_{24}, the spatial arrangement of boron atoms is crucial. At an impurity concentration of 15 %, the average charge on boron atoms is 0.308. When switching to a concentration of 25 %, two options are possible: a decrease in this indicator by 19.8 % for type A and an increase by 6.4 % for type B. The difference in the value of the average charge on boron atoms for the two types of structures is 24.9 %. The average charge on carbon atoms decreases from -0.062 for BC_5 to -0.082 for BC_3 C_{24} type A and -0.110 for type B. In the case of a 50 % impurity concentration, the average charge on boron atoms is 0.243 for type A and 0.257 for type B; here, too, the minimum average charge on carbon atoms for all considered C_{24}-based structures

FIG. 8. One-electron spectra and total DOS of the C$_{24}$ (a), total DOS (green curve) and partial DOS of boron atoms (blue curve) of the BC$_5$ C$_{24}$ (b), BC$_3$ C$_{24}$ type A (c), BC$_3$ C$_{24}$ type B (d), BC C$_{24}$ type A (e), BC C$_{24}$ type B (f)
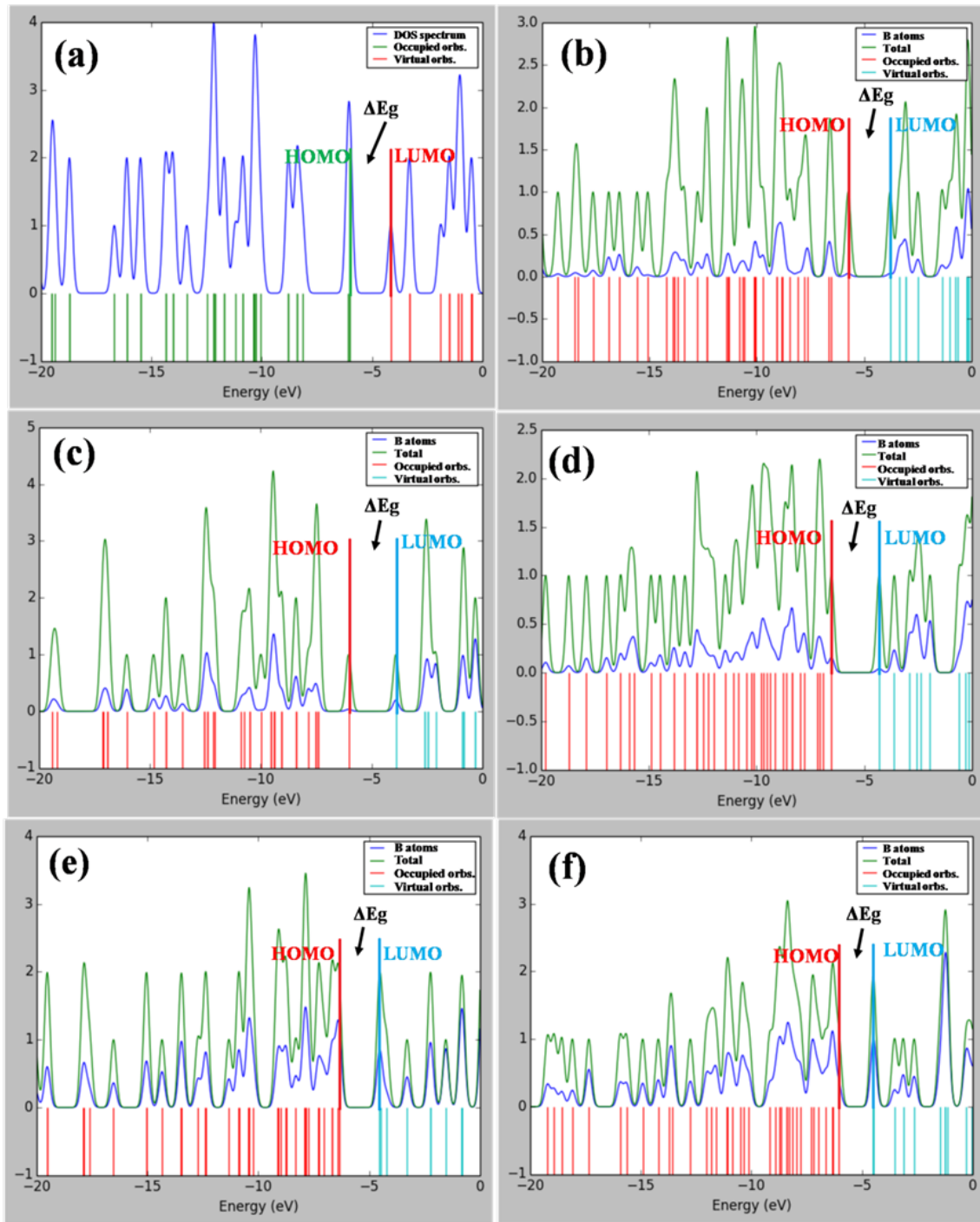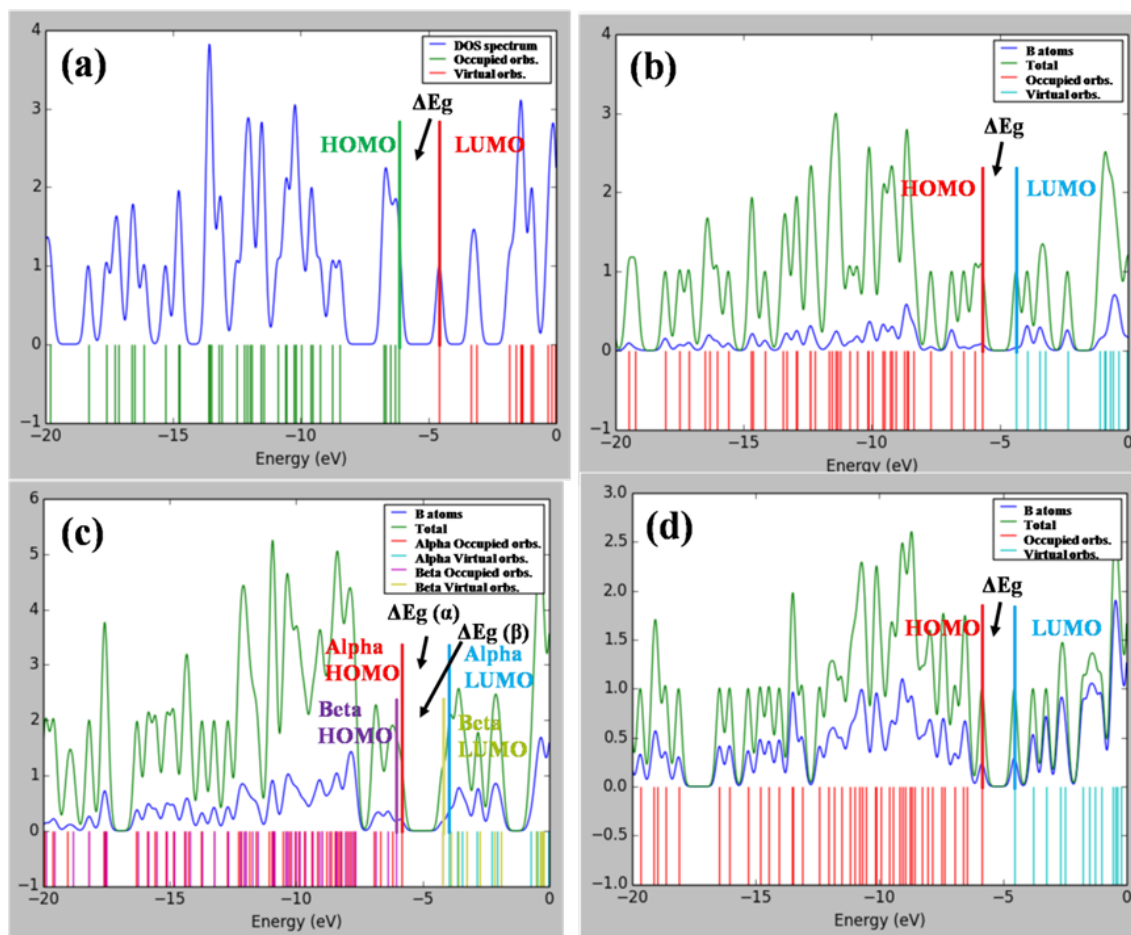
FIG. 9. One-electron spectra and total DOS of the C_{28} (a), total DOS (green curve) and partial DOS of boron atoms (blue curve) of the BC_5 C_{28} (b), BC_3 C_{28} (c), BC C_{28} (d)

is -0.243 for type A and -0.257 for type B. In the case of fullerene C_{28}, the maximum average charge on boron atoms is for the BC_3 structure and is 0.337; for BC_5 and BC, the values of this parameter are 0.334 and 0.263, respectively. The average charge on carbon atoms decreases monotonously from -0.056 for BC_5 to -0.263 for BC.

Table 1 presents a compilation of the values of all the physical quantities discussed in the work.

4. Conclusion

In the present work optimized structures of boron doped small fullerenes C_{20}, C_{24}, and C_{28} with concentrations of the impurity of boron atoms of 15, 25, and 50 % were obtained. The study of their stability, geometric and electronic properties was carried out by calculations performed using methods of DFT. Single-electron spectra and DOS were also obtained for all the structures considered.

Thus, it was found that small fullerenes doped with boron atoms remain stable enough for their practical production. In the vast majority of cases, the substitution of carbon atoms with boron atoms leads to a decrease in the length of the C–C bond. At the same time, the B–C and B–B bonds formed have a longer length compared to C–C. The doping of the fullerene C_{28} with 50 % of the boron atoms impurity leads to a sufficiently strong distortion of its geometric structure and the appearance of octagons in it.

The possibility of obtaining materials with different band gap widths from 1.311 to 3.007 eV by doping of the considered small fullerenes with different concentrations of boron atoms was established. The change in this parameter is associated with the restructuring of the electronic structure, the displacement of the bottom of the conduction band and the top of the valence band. If in fullerenes C_{20} and C_{24} the determining process leading to a decrease in the band gap was a decrease in the bottom of the conduction band, then in the case of fullerene C_{28} this was determined by an increase in the top of the valence band. For all the considered nanostructures, it was established that the addition of 50 % of the impurity of boron atoms leads to a decrease in the band gap. This may be due to the fact that the average charge on carbon atoms and boron atoms in them is equal in modulus.

Ultimately, the present work demonstrated the possibility of controlling the refractive index of nanomaterials based on small fullerenes by changing the band gap by doping the material with boron atoms. Thus, it is possible to construct

TABLE 1. Geometric and electronic properties of boron doped small fullerenes C_{20}, C_{24}, C_{28}. $d_{C–C}$ – an average length of the C–C bond, $d_{B–C}$ – an average length of the B–C bond, $d_{B–B}$ – an average length of the B–B bond, E_b – binding energy, E_{LUMO} – energy of the lowest unoccupied molecular orbital, E_{HOMO} – energy of the highest occupied molecular orbital, ΔE_g – band gap, $Q(C)$ – an average charge on carbon atoms, $Q(B)$ – an average charge on boron atoms

Structure	$d_{C–C}$, Å	$d_{B–C}$, Å	$d_{B–B}$, Å	E_b, eV	E_{LUMO}, eV	E_{HOMO}, eV	ΔE_g, eV	$Q(C)$	$Q(B)$
C_{20}	1.4636	—	—	155.67	–3.568	–5.401	1.833	0.000	—
BC5 C_{20}	1.4636	1.5627	—	148.48	–3.254 (α) –4.512 (β)	-6.261 (α) –6.471 (β)	3.007 (α) 1.959 (β)	–0.055	0.313
BC$_3$ C_{20}	1.4578	1.5883	—	142.71	–4.034 (α) –5.013 (β)	–6.719 (α) –6.726 (β)	2.685 (α) 1.713 (β)	–0.086	0.258
BC C_{20} type A	1.4387	1.5851	1.7120	124.15	–4.208	–5.725	1.517	–0.242	0.242
BC C_{20} type B	1.4247	1.5881	1.7056	124.43	–4.384	–6.022	1.638	–0.238	0.238
C_{24}	1.4651	—	—	190.22	–4.146	–6.010	1.864	0.000	—
BC$_5$ C_{24}	1.4725	1.5448	—	179.13	–3.791	–5.741	1.950	–0.062	0.308
BC$_3$ C_{24} type A	1.4586	1.5703	—	175.07	–3.900	6.030	2.130	–0.082	0.247
BC$_3$ C_{24} type B	1.4543	1.5773	—	175.46	–4.305	–6.521	2.216	–0.110	0.329
BC C_{24} type A	1.4334	1.5778	1.7409	152.10	–4.555	–6.356	1.801	–0.243	0.243
BC C_{24} type B	1.4349	1.5860	1.6942	151.45	–4.522	–6.053	1.531	–0.257	0.257
C_{28}	1.4579	—	—	225.95	–4.569	–6.157	1.588	0.000	—
BC$_5$ C_{28}	1.4575	1.5631	—	214.13	–4.359	–5.687	1.328	–0.056	0.334
BC$_3$ C_{28}	1.4556	1.5713	—	206.03	–3.948 (α) –4.227 (β)	–5.844 (α) –6.054 (β)	1.896 (α) 1.827 (β)	–0.112	0.337
BC C_{28}	1.4043	1.5638	2.6052	182.82	–4.541	–5.852	1.311	–0.263	0.263

heterostructures in general and photonic crystals in particular based on considered nanostructures. This opens up new opportunities for creating new and improving existing optoelectronic devices that can find their application in modern infocommunication systems.

References

[1] Essiambre R.J., Tkach R.W. Capacity trends and limits of optical communication networks. *Proceedings of the IEEE*, 2012, **100** (5), P. 1035–1055.

[2] El-Hageen H.M., Alatwi A.M., Zaki Rashed A.N. High-speed signal processing and wide band optical semiconductor amplifier in the optical communication systems. *J. of Optical Communications*, 2024, **44** (sl), s1277–s1284.

[3] Soma D., Beppu S., Wakayama Y., Sumita S., Takahashi H., Yoshikane N., Morita I., Fellow, Tsuritani T., Suzuki M. 50.47-Tbit/s standard cladding coupled 4-core fiber transmission over 9,150 km. *J. of Lightwave Technology*, 2021, **39** (22), P. 7099–7105.

[4] Manral A., Singh R. Lifi technology. *Int. J. of Scientific Research in Science, Engineering and Technology*, 2016, **2**, P. 493–498.

[5] Khaleel B.M., Alatba S.R., Hamdoun S.H., Terenchuk S. Exploring Li-Fi for IoT Advanced Audio Data Transfer. *Proceedings of the Conference "35th Conference of Open Innovations Association (FRUCT)"*, Tampere, Finland, 9 May 2024, P. 343–351.

[6] Alfattani S. Review of LiFi technology and its future applications. *J. of Optical Communications*, 2021, **42** (1), P. 121–132.

[7] Oton E., Cigl M., Morawiak P., Mironov S., Bubnov A., Piecek W. All-optical 3D blue phase photonic crystal switch with photosensitive dopants. *Scientific Reports*, 2024, **14** (1), 9910.

[8] Masilamani S., Samundiswary P. Compact and efficient PC-based directional coupler all-optical switch. *J. of Optical Communications*, 2024, **44** (s1), s153–s160.

[9] Kumar V., Suthar B. Unit cell independent optical filter using one-dimensional photonic crystal. *J. of Optics*, 2024, **53**, P. 5106–5109.

[10] Banerjee A. Design of an optical buffer by using 1D quaternary photonic crystal. *J. of Optics*, 2024, **53** (2), P. 817–820.

[11] Zhang A., Yang X., Wang J. Design of Channel Drop Filters Based on Photonic Crystal with a Dielectric Column with Large Radius inside Ring Resonator. *Photonics*, 2024, **11** (6), 554.

[12] Liu M.D., Chen H.H., Wang Z., Zhang Y., Zhou X., Tang G.J., Ma F., He X.T., Chen X.D., Dong J.W. On-Chip Topological Photonic Crystal Nanobeam Filters. *Nano Letters*, 2024, **24** (5), P. 1635–1641.

[13] Wang Y., Yao Y., Zhang H., Liu B., Duan S., Lin W. An electrically controlled tunable photonic crystal filter based on thin-film lithium niobate. *Optoelectronics Letters*, 2024, **20** (4), P. 200–204.

[14] Ankita, Suthar B., Bissa S., Bhargava A. Dual-channel optical filter based on photonic crystal with double defect. *J. of Optics*, 2024, **53**, P. 3996–3999.

[15] Hazra S., Mukhopadhyay S. Photonic crystal based integrated system for half adder and half subtractor operations. *Optical and Quantum Electronics*, 2024, **56** (5), 855.

[16] Pathak P., Zafar R., Kanungo V., Vyas S. Photonic crystal-based all-optical half adder with high contrast ratio. *J. of Optical Communications*, 2024, **44** (s1), s119–s124.

[17] Hazra S., Mukhopadhyay S. Implementation of photonic crystal based optical full adder using ring resonators. *Optics Communications*, 2024, 130828.

[18] Goswami K., Mondal H., Sen M. Design of all optical logic half adder based on holes-in-slab photonic crystal. *Optical and Quantum Electronics*, 2024, **56** (2), 271.

[19] Askarian A. All optical half subtractor based on linear photonic crystals and phase shift keying technique. *J. of Optical Communications*, 2024, **44** (s1), s449–s455.

[20] Chen H., Chen H., Li A., Liu M., Chan E.H.W. Simple and reconfigurable photonics-based half adder and half subtracter. *Optics Communications*, 2024, **555**, 130206.

[21] Elhachemi K., Rafah N. A novel proposal based on 2D linear resonant cavity photonic crystals for all-optical NOT, XOR and XNOR logic gates. *J. of Optical Communications*, 2024, **44** (s1), s283–s291.

[22] He L., Liu D., Zhang H., Zhang F., Zhang W., Feng X., Huang Y., Cui K., Liu F., Zhang W., Zhang X. Topologically Protected Quantum Logic Gates with Valley-Hall Photonic Crystals. *Advanced Materials*, 2024, **36** (24), 2311611.

[23] Mitin V.V., Kochelap V.A., Stroscio M.A. *Quantum heterostructures: microelectronics and optoelectronics*. Cambridge: University Press, Cambridge, 1999, 642 p.

[24] Yablonovitch E. Photonic band-gap structures. *JOSA B*, 1993, **10** (2), P. 283–295.

[25] Yang Y., Wang L., Yang H., Li Q. 3D chiral photonic nanostructures based on blue-phase liquid crystals. *Small Science*, 2021, **1** (6), 2100007.

[26] Vlasov Y.A., O'Boyle M., Hamann H.F., McNab S.J. Active control of slow light on a chip with photonic crystal waveguides. *Nature*, 2005, **438** (7064), P. 65–69.

[27] Gersen H., Karle T.J., Engelen R.J.P., Bogaerts W., Korterik J.P., van Hulst N.F., Krauss T.F., Kuipers L. Real-space observation of ultraslow light in photonic crystal waveguides. *Physical Review Letters*, 2005, **94** (7), 073903.

[28] Kempa K., Kimball B., Rybczynski J., Huang Z.P., Wu P.F., Steeves D., Sennett M., Giersig M., Rao D.V.G.L.N., Carnahan D.L., Wang D.Z., Lao J.Y., Li W.Z., Ren Z.F. Photonic crystals based on periodic arrays of aligned carbon nanotubes. *Nano Letters*, 2003, **3** (1), P. 13–18.

[29] Cui K., Lemaire P., Zhao H., Savas T., Parsons G., Hart A.J. Tungsten–carbon nanotube composite photonic crystals as thermally stable spectral-selective absorbers and emitters for thermophotovoltaics. *Advanced Energy Materials*, 2018, **8** (27), 1801471.

[30] Sun X., Zhang J., Lu X., Fang X., Peng H. Mechanochromic photonic-crystal fibers based on continuous sheets of aligned carbon nanotubes. *Angewandte Chemie Int. Ed.*, 2015, **54** (12), P. 3630–3634.

[31] Tan Y.C., Tou Z.Q., Mamidala V., Chow K.K., Chan C.C. Continuous refractive index sensing based on carbon-nanotube-deposited photonic crystal fibers. *Sensors and Actuators B: Chemical*, 2014, **202**, P. 1097–1102.

[32] Butt H., Dai Q., Wilkinson T.D., Amaratunga G.A.J. Negative index photonic crystal lenses based on carbon nanotube arrays. *Photonics and Nanostructures – Fundamentals and Applications*, 2012, **10** (4), P. 499–505.

[33] Mahmoodi Y., Fathi D. High-performance refractive index sensor for oil derivatives based on MWCNT photonic crystal microcavity. *Optics & Laser Technology*, 2021, **138**, 106865.

[34] Soolookinejad G., Payravi M., Jabbari M., Nafar M., Sangachin E.A. Optical multistability in 1D photonic crystal doped with carbon-nanotube quantum dot nanostructures. *Laser Physics*, 2017, **27** (12), 125202.

[35] Fernandes J.A., Feitosa F.A.O., Costa C.H.O., Vasconcelos M.S., Bezerra C.G., Anselmo D.H.A.L. Graphene-embedded planar and cylindrical Oldenburger–Kolakoski aperiodic photonic crystals. *Optical Materials*, 2024, **148**, 114832.

[36] Hossain M.M., Talukder M.A. Tamm and surface plasmon hybrid modes in anisotropic graphene-photonic-crystal structure for hemoglobin detection. *Optics Express*, 2024, **32** (8), P. 14261–14275.

[37] Xia B., Zeng X., Lan W., Zhang M., Huang W., Wang H., Liu C. Cellulose nanocrystal/graphene oxide one-dimensional photonic crystal film with excellent UV-blocking and transparency. *Carbohydrate Polymers*, 2024, **327**, 121646.

[38] Kumar C., Raghuwanshi S.K., Kumar V. Graphene-based patch antenna array on photonic crystal substrate at terahertz frequency band. *J. of Electromagnetic Waves and Applications*, 2024, **38** (2), P. 250–263.

[39] Liu W., Li G., Chen C., Liu J., Li Z.Y. Broadly tunable filter based on a graphene MEMS-photonic crystal composite structure and its application in single-pixel full-color displays. *J. of Materials Chemistry C*, 2024, **12** (18), P. 6588–6595.

[40] Elblbeisi M., Taya S.A., Almawgani A.H., Hindi A.T., Alhamss D.N., Colak I., Patel S.K. Absorption Properties of a Defective Binary Photonic Crystal Consisting of a Metamaterial, SiO_2, and Two Graphene Sheets. *Plasmonics*, 2024, **19** (3), P. 1431–1442.

[41] Zhang C., Ota Y., Iwamoto S. Wide-mode-area slow light waveguides in valley photonic crystal heterostructures. *Optical Materials Express*, 2024, **14** (7), P. 1756–1766.

[42] Kislyakov I.M., Ivanov P.V., Nunzi J.M., Vlasov A.Y., Ryzhov A.A., Venediktova A.V., Wang H., Wang Z., Zhang T., Dong N., Wanget J. Nonlinear optical fullerene and graphene-based polymeric 1D photonic crystals: perspectives for slow and fast optical bistability. *JOSA B*, 2021, **38** (9), C198–C$_2$09.

[43] Gaevski M.E., Kognovitskii S.O., Konnikov S.G., Nashchekin A.V., Nesterov S.I., Seisyan R.P., Zadiranov J.M. Two-dimensional photonic crystal fabrication using fullerene films. *Nanotechnology*, 2000, **11** (4), 270.

[44] Xu B., Han P., Wang L., Li J., Liu X., Chen M., Hideki I. Optical properties in 2D photonic crystal structure using fullerene and azafullerene thin films. *Optics communications*, 2005, **250** (1–3), P. 120–125.

[45] Srivastava S., Ojha S. Omnidirectional reflection bands in one-dimensional photonic crystal structure using fullerene films. *Progress In Electromagnetics Research*, 2007, **74**, P. 181–194.

[46] Belousova I.M., Ryzhov A.A. Numerical simulation of nonlinear properties of fullerene-containing one-dimensional photonic crystal. *Optics and Spectroscopy*, 2012, **112**, P. 902–905.

[47] Sawant S.V., Patwardhan A.W., Joshi J.B., Dasgupta K. Boron doped carbon nanotubes: Synthesis, characterization and emerging applications – A review. *Chemical Engineering J.*, 2022, **427**, 131616.

[48] Zhang J.J., Ma J., Feng X. Precision Synthesis of Boron-Doped Graphene Nanoribbons: Recent Progress and Perspectives. *Macromolecular Chemistry and Physics*, 2023, **224** (1), 2200232.

[49] Zaporotskova I.V., Boroznin S.V., Belonenko M.B., Drychkov E.S., Butenko Y.V. Graphene Nanotapes Modified with Impurity Boron Atoms as a Basis for Two-Dimensional Photonic Crystals. *Bulletin of The Russian Academy of Sciences: Physics*, 2022, **86**, P. 1450–1453.

[50] Zaporotskova I.V., Boroznina N.P., Boroznin S.V., Drychkov E.S., Butenko Y.V., Belonenko M.B. Carbon Nanotubes Doped with Boron as a Basis for Two-Dimensional Photonic Crystals. *Bulletin of The Russian Academy of Sciences: Physics*, 2022, **86**, P. 673–677.

[51] Boroznin S.V., Carbon nanolayers modified with boron atoms as a basis for devices with ionic conductivity: theoretical study. *J. of Advanced Materials and Technologies*, 2022, **7** (2), P. 97–103.

[52] Fuentes G.G., Borowiak-Palen E., Knupfer M., Pichler T., Fink J., Wirtz L., Rubio A. Formation and electronic properties of BC_3 single-wall nanotubes upon boron substitution of carbon nanotubes. *Physical Review B—Condensed Matter and Materials Physics*, 2004, **69** (24), 245403.

[53] Yang N., Liu G., Chen T., Dong X., Li Y., Xu Z. Unveiling adsorption characteristics of BC5 monolayer: High electronic anisotropy and gas sensing performance. *Applied Surface Science*, 2023, **615**, 156226.

[54] Chuvilin A., Kaiser U., Bichoutskaia E., Besley N.A., Khlobystov A.N. Direct transformation of graphene to fullerene. *Nature Chemistry*, 2010, **2** (6), P. 450–453.

[55] Koch W., Holthausen M., *A Chemist's Guide to Density Functional Theory*, Wiley-VCH, Weinheim, 2002, 306 p.

[56] Sakr M.A., Abdelsalam H., Teleb N.H., Abd-Elkader O.H., Zhang Q. Exploring the structural, electronic, and hydrogen storage properties of hexagonal boron nitride and carbon nanotubes: insights from single-walled to doped double-walled configurations. *Scientific Reports*, 2024, **14** (1), 4970.

[57] Tomilin O.B., Rodionova E.V., Rodin E.A., Knyazev A.V. Emission properties of boron and nitrogen doped ultrashort carbon nanotubes. *Applied Surface Science*, 2024, **669**, 160443.

[58] Pei S., Li J., Bai Z., Wang C., Lv X. Atomic insights of structural, electronic properties of B, N, P, S, Si-doped fullerenes and lithium ion migration with DFT-D method. *J. of Molecular Modeling*, 2024, **30** (12), 422.

[59] Kurban M. Electronic structure, optical and structural properties of Si, Ni, B and N-doped a carbon nanotube: DFT study. *Optik*, 2018, **172**, P. 295–301.

[60] O'boyle N.M., Tenderholt A.L., Langner K.M. Cclib: a library for package-independent computational chemistry algorithms. *J. of Computational Chemistry*, 2008, **29** (5), P. 839–845.

[61] North S.C., Jorgensen K.R., Pricetolstoy J., Wilson A.K. Population analysis and the effects of Gaussian basis set quality and quantum mechanical approach: main group through heavy element species. *Frontiers in Chemistry*, 2023, **11**, 1152500.

Information about the authors:

Anton R. El Zanin – Volgograd State University, Universitetskiy av., 100, Volgograd, 400062, Russia;
ORCID 0009-0005-3897-9490; aelzanin@volsu.ru

Sergey V. Boroznin – Volgograd State University, Universitetskiy av., 100, Volgograd, 400062, Russia;
ORCID 0000-0003-0110-2271; boroznin@volsu.ru

Irina V. Zaporotskova – Volgograd State University, Universitetskiy av., 100, Volgograd, 400062, Russia;
ORCID 0000-0002-9486-2482; zaporotskova@volsu.ru

Conflict of interest: the authors declare no conflict of interest.